Desalination and Water Treatment
www.deswater.com

doi: 10.5004/dwt.2018.21739

109 (2018) 221–230
March

Characterization of hydrogen peroxide (H_2O_2) modified hydrochars from walnut shell for enhanced adsorption performance of methylene blue from aqueous solution

Yang Huang[a], Yan Huang[b,*], Weiqing Wang[a], Kui Zheng[c]

[a]*Laboratory of Solid Waste Treatment and Resource Recycle, Ministry of Education, Mianyang 621010, China, Tel. +86 816 2419223; Fax: +86 816 6089453; emails: swusthy@163.com (Y. Huang), swustwwq@sohu.com (W. Wang)*
[b]*School of Life Science and Technology, Southwest University of Science and Technology, Mianyang 621010, China, Tel. +86 816 2419223; Fax: +86 816 6089453; email: hyswust@163.com (Y. Huang)*
[c]*Analytical and Testing Center, Southwest University of Science and Technology, Mianyang 621010, China, Tel. +86 816 6089508; Fax: +86 816 6089508; email: 77651416@qq.com*

Received 10 July 2017; Accepted 25 November 2017

ABSTRACT

Hydrothermal carbonization of waste biomass materials is becoming more prevalent in the production of carbonaceous adsorbents. In this work, mesoporous hydrochars were prepared by the hydrothermal carbonization of walnut shell (HTC-WS) as novel adsorbents of methylene blue (MB) from aqueous solution. In order to enhance the adsorption ability, HTC-WS was chemically modified using H_2O_2. Both materials were characterized by elemental analysis, Fourier transform infrared spectroscopy, scanning electron microscope, zeta potential analysis and nitrogen adsorption–desorption measurements. Additionally, the adsorption performances of these two hydrochars toward MB were evaluated. The results showed that H_2O_2 modification of hydrochars might have increased the oxygen-containing functional groups, such as carboxyl groups, resulting in more than three times increase of MB adsorption capacity (173.92 mg/g) compared with unmodified hydrochars (50.56 mg/g). MB adsorption kinetics of HTC-WS and hydrothermal carbonization of H_2O_2-activated walnut shell could be interpreted with pseudo-second-order models and adsorption equilibrium data were best fitted by the Langmuir isotherm model. Oxygenated functional groups of these two hydrochars were significant adsorption sites and appeared to be associated with molecular electrostatic interactions between MB and hydrochars. The results suggested that H_2O_2 modified hydrochars were environmental friendly, effective and low-cost adsorbents for the removal of MB from wastewater.

Keywords: Walnut shell; Hydrothermal carbonization; Hydrogen peroxide; Methylene blue; Adsorption

1. Introduction

Hydrothermal carbonization (HTC) has received growing attentions in recent years as a viable technology for conversion of biomass materials to carbonaceous products [1]. The biomass in HTC process are heated at relatively low temperatures (180°C–350°C) and decomposed in a closed reactor under autogenous pressures to produce solid hydrochars [2–4]. The formation of hydrochars is a result of hydrolysis, condensation, decarboxylation and dehydration reactions [5]. Compared with the traditional pyrolyzed biochar, the feedstock in HTC process does not need to be dried. Additionally, hydrochar has a lower carbon content and higher degree reactive oxygen functional groups (e.g., hydroxyl and carboxylic) than that of pyrolysis biochar, making it act as an effective lower cost adsorbent for environmental pollutants [6]. Furthermore, hydrochars have been widely applied as cheap raw materials for porous carbon, catalysts

* Corresponding author.

supports, electrode materials and wastewater adsorbents [7]. As adsorbents for decontamination of wastewater, previous studies demonstrated that hydrochars had the potential to remove organics and heavy metals from aqueous solution [8,9].

Generally, biochar produced at high temperature (400°C–700°C) shows higher adsorption capacity due to having greater surface area and microporosity [10]. However, the biomass in HTC process was usually heated at relatively mild conditions (180°C–350°C), which indicated that hydrochars may have a relatively low surface area, poor porosity and low adsorption capacity [11]. In order to further enhance the adsorption ability of hydrochars, several activating agents have been used to modify the hydrochar's surface structure, such as KOH, NaOH and H_2O_2 [3,12–14]. Some studies have demonstrated that alkali modification (KOH, NaOH) could increase the aromatic and oxygen-containing functional groups on hydrochar surface, which subsequently improved organics and heavy metals adsorption capacity of activated hydrochars [13,15–17]. Compared with the strong alkaline, H_2O_2 is relatively inexpensive and clean, which is favorable for popularization and application. For example, Zuo et al. [18] investigated the removal of the Cu(II) from the solution using untreated and H_2O_2-activated hydrochars from peanut hull; the results showed that the content of oxygen functional groups on hydrochar surface was enhanced by the H_2O_2 modification, which results in an increase of 30% adsorption ability of H_2O_2-activated hydrochars in comparison with that of the untreated material. Xue et al. [14] reported that activation of hydrochars obtained from *Cymbopogon schoenanthus* L. Spreng using H_2O_2 has significantly improved hydrochar's adsorption capacities for Pb^{2+}. To the best of our knowledge, although hydrochars have been extensively studied to analyze the adsorption of metal ion, the study of the adsorption of organic pollutants onto H_2O_2-activated hydrochars is few.

Raw material of hydrochars is always obtained from some waste biomass materials, such as the husks of cereal, food waste, sawdust and other agricultural waste, which are abundant, sustainable, renewable and environmental friendly resources for preparation of hydrochars [1,19]. Walnut is a conventional economic crop in China and the annual output of walnut has exceeded 1 million tons. A large number of walnut shells were discarded as agricultural waste or were burned as domestic fuel every year. Walnut shell contains high fraction of lignin, cellulose and hemicellulose as the potential material for char production. Now, previous studies have reported that biochars were produced using walnut shell by pyrolysis under anaerobic or anoxic conditions [20–22]. To our knowledge, few studies have examined that hydrochars were prepared using walnut shell by HTC.

In this study, hydrothermal carbonization of walnut shell (HTC-WS) and their H_2O_2-activated form (HTC-AWS) were prepared and characterized. The adsorption potentials of HTC-WS and HTC-AWS for methylene blue (MB) (a cationic dye which was selected as artificially organic pollutant) removal was evaluated. The effects of various factors on the adsorption such as initial pH, adsorbent dosage, contact time and initial MB concentration had been investigated in this study. The equilibrium and kinetic data of the adsorption studies were processed to understand the adsorption mechanism of MB onto walnut shell-hydrochar.

2. Materials and methods

2.1. Materials preparation and characterization

Walnut was purchased at local market. The walnut shell was removed from walnut and the collected waste walnut shell was washed with distilled water, dried under 105°C for 24 h. Afterwards, the walnut shell was crushed in a knife-mill and sieved until all particle diameter were lower than 150 μm. The obtained walnut shell powder was preserved in the desiccator and used in the following studies. To prepare hydrothermally carbonized walnut shell, 10 g of walnut shell powder and 10 mg of citric acid (as a catalyst for carbonization) in 70 mL of water were subjected to HTC in a 100 mL Teflon-lined stainless steel autoclave at 180°C for 6 h. The product was then separated from the liquid phase and washed with distilled water, dried under 105°C for 24 h. The resulting material HTC-WS was used as an adsorbent. Further treatment of HTC-WS with H_2O_2 in water was carried out in a method similar to that reported by Hammud et al. [23]. Briefly, 3 g of the HTC-WS were immersed in 20 mL of H_2O_2 solution (10%) for 2 h. The suspension was then kept in 80°C water bath for 24 h. The obtained product (HTC-AWS) was washed with distilled water and dried at 105°C for 24 h. HTC-WS and HTC-AWS were ground and sieved to less than 75 μm to be used for adsorption experiments. MB used was of analytical grade.

2.2. Characterization of adsorbent

Elemental analysis measurements of carbon, hydrogen and nitrogen content were recorded using a Vario EL CUBE elemental analyzer and oxygen contents were determined by difference. Fourier transform infrared spectroscopy (FT-IR) spectrum was acquired by PerkinElmer Fourier transform infrared spectroscopy, the spectrum ranged from 4,000 to 400 cm^{-1}. Morphology analysis was performed on Scanning Electron Microscope (SEM) Stereoscan 440 Leica. Zeta potential of the materials was determined by microelectrophoresis using Malvern Zetasizer Nano ZS90 zeta potential analyzer. The zeta potentials of the materials suspensions containing 0.5% solid in 0.01 mol L^{-1} $NaNO_3$ were determined at various pH values. A nitrogen adsorption system (Quantachrome, Autosorb-1MP) was employed to record the adsorption–desorption isotherms at the liquid-nitrogen temperature of 77 K.

2.3. Adsorption experiments

For each adsorption experiment, walnut shell-derived hydrochars (HTC-WS or HTC-AWS) and MB solution of known concentration were transferred in 100 mL flask, and shaken at 25°C in a controlled shaker at a constant speed of 150 rpm with a required adsorption time and required pH. Initial MB concentrations for HTC-WS and HTC-AWS were fixed to be 50 and 100 mg/L, respectively, when the effects of solution initial pH values, adsorbent dosage, contact time were investigated, because the adsorption capacity of the two adsorbents was different. The effect of pH was performed by dispersion of 0.02 g of adsorbent in 25 mL of MB solution. Effect of solution pH on adsorption of MB was investigated in the range of 2.0–11.0 by the addition of 0.1 mol/L H_2SO_4

or 0.1 mol/L NaOH solutions. The adsorbent dosage was changed from 0.4 to 2 g/L in order to investigate the influence of dosage of walnut shell-hydrochar. The adsorption kinetics was determined by analyzing adsorption capacity from the aqueous solution at 0–360 min. For adsorption isotherms, MB solution concentrations for HTC-WS and HTC-AWS were in the range of 10–100 mg/L and 50–200 mg/L, respectively. The samples were separated from mixture solution by centrifugation with a speed of 4,000 rpm for 10 min. The concentrations of MB were measured with Thermo Fisher Evolution EV300 UV–visible spectrophotometer at appropriate wavelengths corresponding to the maximum absorbance of MB, 662 nm. The adsorbed amounts (q) of MB were calculated by the following equation:

$$q = \frac{(C_0 - C_e) \times V}{m} \quad (1)$$

where C_0 and C_e are the initial and equilibrium concentrations of MB (mg/L), V is the volume of solution (L) and m is the mass of adsorbent (g).

3. Results and discussion

3.1. Characterization of the adsorbent

The elemental analysis of the walnut shell (WS), HTC-WS and HTC-AWS is presented in Table 1 to show significant changes caused by HTC process and H_2O_2 treatment. The results indicated that all these hydrochars (HTC-WS and HTC-AWS) and the feedstock had high carbon contents (48.381%–57.985%). The HTC process increased the carbon content and reduced H content and O content of the two hydrochars compared with that of WS, which might be caused by hydrolysis, condensation, decarboxylation and dehydration reactions [5]. Elemental compositions analysis showed that elemental compositions among the HTC-WS and HTC-AWS were similar, indicating stability of hydrochar by the treatment of H_2O_2. However, the O/C and H/C ratios of HTC-AWS (0.757, 0.086) were higher than that of HTC-WS (0.636, 0.085), which might make them better adsorbents for aqueous contaminants [16]. Additionally, the high O/C and H/C elemental ratios of HTC-AWS indicated a low degree of carbonization of WS at 180°C hydrothermal conditions, and also implied a high content of non-carbonizable organic matters in the HTC-AWS.

FT-IR analysis revealed the difference in the functionality of the WS and hydrochars products as shown in Fig. 1(a). FT-IR spectrum of WS represented the spectrum bands of ν(O–H) and ν(N–H) at 3,341 cm^{-1}, ν(C–H) at 2,930 cm^{-1}, ν(C=O) at 1,730 cm^{-1}, ν(C=C) at 1,597 cm^{-1}. In general, the FT-IR spectrum of WS was complex because it consisted of several kinds of organic matters, and their absorption peak incorporated was obvious. The band 3,341 cm^{-1} was attributed to the hydroxyl groups in phenolic and aliphatic structures. The band 2,930 cm^{-1} was C–H stretching in aromatic methoxyl groups and methylene groups of side chains. The band of the carbonyl group in ketones, aldehydes or carboxyl appears at 1,730 cm^{-1}. The band at 1,597 cm^{-1} may originate from carbohydrates. The bands at 1,160–1,031 cm^{-1} were associated with C–O, C–C stretching and C–OH bending in structure of hydrochars [24]. The FT-IR spectrum of WS was changed by HTC at 180°C. The peaks at 1,607,

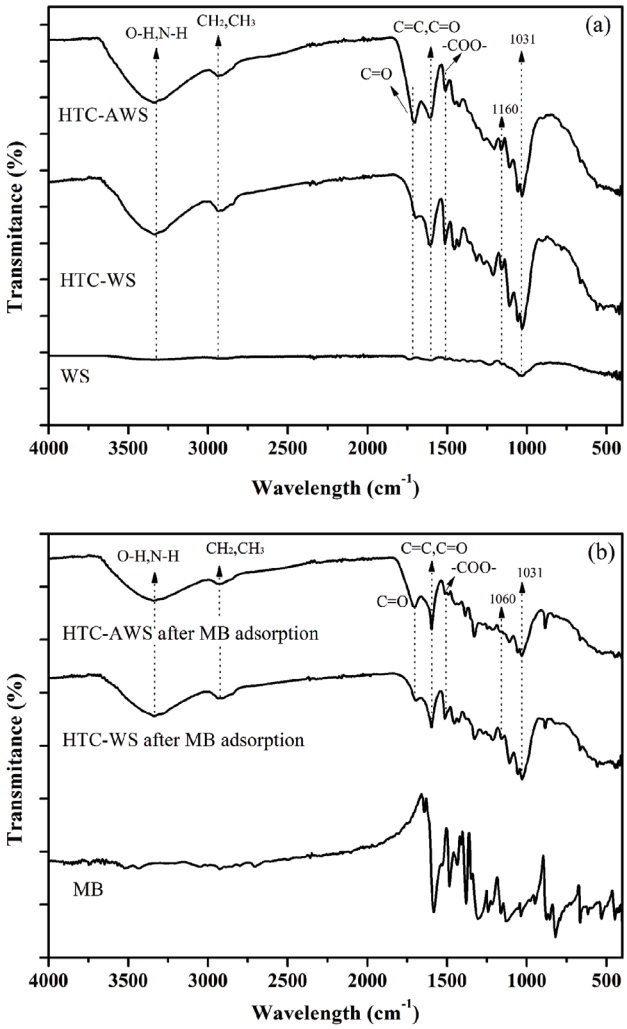

Fig. 1. FT-IR spectrum of (a) walnut shell and hydrochar products, and (b) hydrochar products after MB adsorption.

Table 1
Elemental analysis results of walnut shell, hydrochars products

Biomass and hydrochars	N%	C%	H%	O%	Atomic ratio H/C	Atomic ratio O/C
Walnut shell	0.195	48.381	5.211	46.213	0.955	0.108
HTC-WS	0.211	57.985	4.940	36.864	0.636	0.085
HTC-AWS	0.164	54.187	4.634	41.015	0.757	0.086

1,509, 1,425 cm^{-1} correspond to carboxylic acid functionality, and were increased by HTC. There was also an increase of peak intensity at 1,160–1,031 cm^{-1}. The band at 1,703 cm^{-1}, which was C=O stretching in carboxylic acid functionality, was increased with H_2O_2 treatment. The results showed that the content of organic carbon and oxygen functional groups increased in HTC-WS and especially HTC-AWS. After MB adsorption, the intensity of some peaks at 1,509, 1,703, 1,060 and 1,031 cm^{-1} corresponding to the C=O functional groups decreased significantly (Fig. 1(b)). Therefore, C=O groups were the possible functional groups involved in the interaction between walnut shell-derived hydrochars and MB dye. These results were consistent with previous studies [3,15].

Distribution of WS-derived hydrochars charge has significant and important role on the removal and interaction of various compounds with adsorbent. The adsorbent charge (positive or negative) influences the interaction of surface with solute ions or molecules by changing the mechanism and forces. The zeta potentials of the HTC-WS and HTC-AWS at various pH values are shown in Fig. 2. These results showed that the point of zero charge (PZC) was 2.72. At pH above PZC, zeta potential values of the surface of the HTC-WS were negative over the entire pH range. The zeta potential value of HTC-AWS was even more negative than those of HTC-WS at a same pH value, which might be attributed to the fact that some of the carboxylic groups were located on the surface of the HTC-WS. The surface of HTC-WS and HTC-AWS was negative from pH 2.5–10, indicating that the high tendency of these cationic species for strong adsorption onto the present adsorbent.

It can be seen from Fig. 3 that the surface morphologies of WS changed greatly after HTC. This change in morphology arose from the decomposition of crystalline cellulose and lignin during HTC. After decomposition of these organic matters, small molecular products may leach out from the

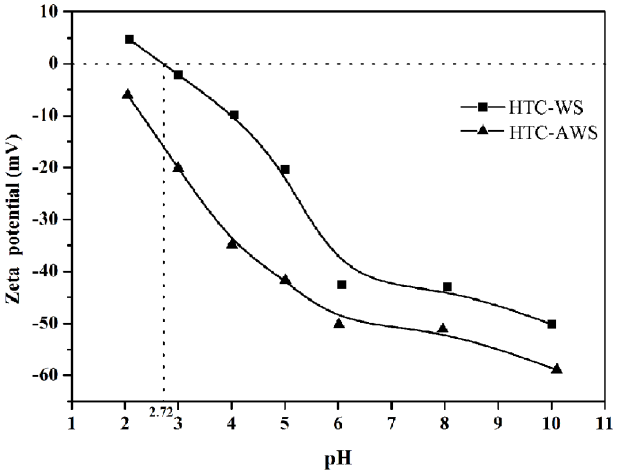

Fig. 2. Zeta potentials of hydrochars products: HTC-WS and HTC-AWS.

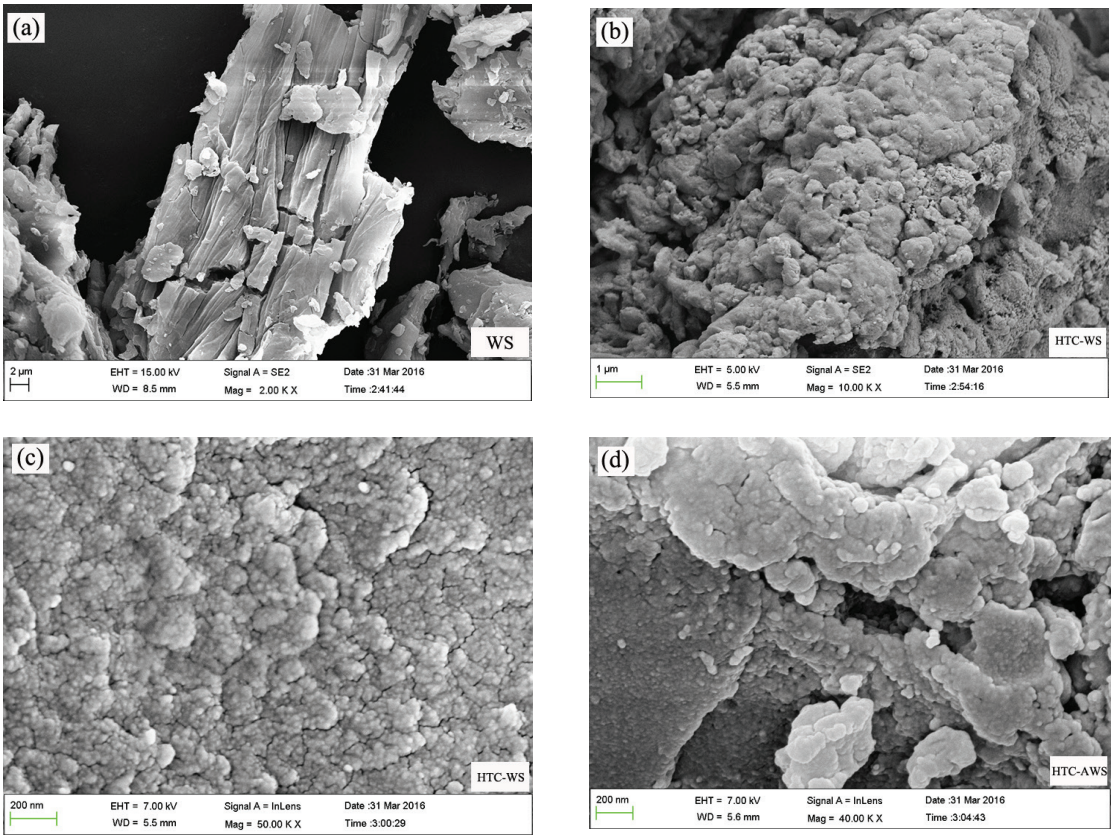

Fig. 3. SEM images of (a) walnut shell, ((b) and (c)) hydrothermally carbonized walnut shell HTC-WS and (d) H_2O_2-activated HTC walnut shell HTC-AWS.

structural matrix, leaving the heterogeneous pores [3]. After chemical activation with H_2O_2, it could be observed that the surface of HTC-AWS was smoother than HTC-WS and had bigger crevices. Similar results of the surface morphologies have been obtained from alkali-modified hydrochar. It speculated that alkali could remove impurities from the partially blocked pores which resulted in an increase of surface cracks [25]. Fig. 3(d) shows that the HTC-AWS had a less porous structure compared with that of HTC-WS (Figs. 3(b) and 3(c)). This finding suggested the effect of H_2O_2 in reducing the pores by destroying porous structure of the materials or blocking pores. The presence of cracks or pores on the surface of hydrochar was an important reason for the adsorption of big molecules of MB, presumably because cracks or pores could provide a larger contact site for MB.

The nitrogen adsorption/desorption isotherms and the corresponding pore size distribution curves of the carbonaceous samples are shown in Fig. 4 and the textural properties are summarized in Table 2. HTC-WS exhibited type IV isotherm in Fig. 4(a), according to the IUPAC classification, which represented the adsorption behavior of mesoporous substances [26]. The calculated Brunauer–Emmett–Teller (BET) surface area of the HTC-WS was 8.01 m^2/g, which was obviously lower than the activated carbon prepared by conventional high temperature carbonization [27]. According to the Barrett–Joyner–Halenda model, the total mesoporous volume was 0.043 cm^3/g, the mesoporous size was in the range of 3.49–134.34 nm. The isotherm types of HTC-AWS were consistent with HTC-WS. However, the hysteresis loop was not obvious in the relative pressure range from 0.4 and 0.9, which indicated that the pore structure of the HTC-AWS had changed. The BET surface area and total mesoporous volume of the HTC-AWS was 3.24 m^2/g and 0.0034 cm^3/g, respectively, which suggested that the porous structure of the surface of the hydrothermal carbon was eluted, oxidized or blocked by H_2O_2. The results also proved that structure of hydrochars from WS by HTC was different from activated carbon by pyrolysis method.

There are some works about the chemical transformations that take place when biomass is treated under hydrothermal condition in the literature [5,7]. According to these results, it is possible to brief the mechanism of the formation of hydrochar products from WS. In a first step, when WS was hydrothermally treated, the lignin, cellulose and hemicellulose hydrolyzed to produce the different oligomers and glucose [7]. Then, the small molecules could be dehydrated or fragmented under the catalysis of H^+ to form hydroxymethyl furfural and other water soluble intermediate products [28]. The following reaction stages were polymerization or condensation reactions to form the soluble polymers. Meanwhile, the aromatization of polymers was in progress. C=O and C=C bonds appear due to the dehydration of intermediates products [29]. When the concentration of polymers in the aqueous solution reaches the critical supersaturation point, nucleation is formed. The nuclei aggregated the chemical species present in the solution by surface diffusion, and finally grew into carbon microspheres containing reactive oxygen functionalities (hydroxyl, carbonyl, carboxylic, etc.) [5]. It could be seen that HTC was a very complicated chemical process, which had great influence on the structure of the product. Treatment with H_2O_2 caused unstable

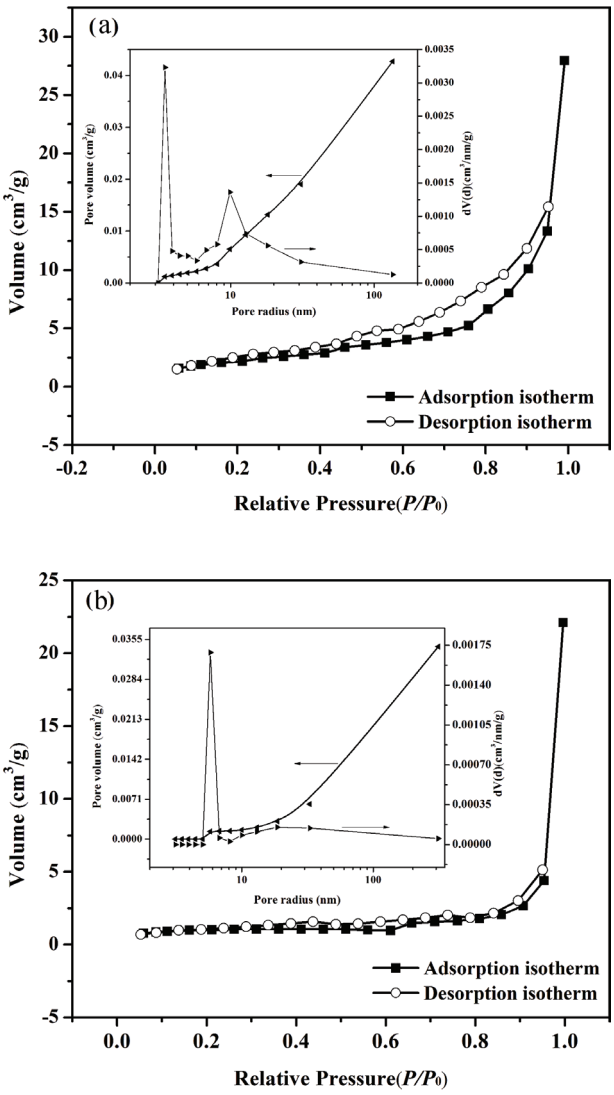

Fig. 4. N_2 adsorption–desorption isotherms of (a) HTC-WS and (b) HTC-AWS. The inset figures show the pore size distributions of the micropores and mesopores.

Table 2
Textural properties of walnut shell-derived hydrochars

Sample	BET surface area (m^2/g)	Total pore volume (cm^3/g)	Micropore volume (cm^3/g)	Mesopore volume (cm^3/g)	Pore size (nm)
HTC-WS	8.01	0.0433	0.0032	0.043	6.988
HTC-AWS	3.24	0.0342	0.0015	0.0034	13.651

functional group to diminish or oxidize into reactive oxygen functionalities with respect to the untreated sample, such as aromatic C=C ring structures [12,30]. Compared with the surface impregnation which is to graft new functional groups on the base [31], the hydrochars modification by H_2O_2 was that improved the hydrochars surface groups. Refer to previous studies [7]; the scheme about the formation of oxygenated functional groups during HTC and H_2O_2 activation was shown in Fig. 5.

3.2. Adsorption of MB onto WS-hydrochar

The initial pH values of the MB solution are important, which control the adsorption process, particularly the adsorption capacity. It can be seen in Fig. 6 that an increase of pH value resulted in an increase of MB removal. At low pH, the quantity adsorbed of HTC-WS for MB was 23.18 mg/g, later on it increased with mounting pH up to 61.93 mg/g. This was happening because the competition decreases between hydrogen ions and the MB cations for the sorption sites of WS-hydrochar [32]. The surface of the HTC-WS was positively charged at pH under 2.72, and showed negative charge over the pH_{PZC}. The MB is a positively charged (cationic) dye and provides positive ions in the solutions [3]. Thus, the electrostatic attraction appeared between negatively charged hydrochar and cationic MB molecules, which should be responsible for the excellent performance for MB adsorption. The quantity adsorbed of HTC-AWS for MB was more than HTC-WS in solution pH from 2 to 11. The reason for strong adsorption capacity of HTC-AWS was presumably that its surface contained excessive acidic functional groups by H_2O_2 as modifying agent according to the FT-IR analysis.

Adsorbent dosage is another important factor influencing MB adsorption. Fig. 7 shows the effect of HTC-WS and HTC-AWS dosage on the MB adsorption capacity. The two hydrochars exhibit a similar trend of decreasing adsorption capacity per unit mass of adsorbent with adsorbent dosage maybe related with the unavailability of the adsorbate sites which were saturated by the MB dye molecule [33]. However, as the adsorbent dosage increased from 0.4 to 2 g/L, the MB removal efficiency increased from 34.51% to 81.03% for HTC-WS, and increased from 55.90% to 99.33% for HTC-AWS, when the initial concentration of MB solution was 50 and 100 mg/L, respectively. The reason was that increasing the absorbent dosage provided more functional groups and active sites, thus leading to the increase in the removal efficiency of MB [34]. In the further experiments, the adsorbent dosage was fixed at 0.8 mg/L.

The effect of the contact time on adsorption of is illustrated in Fig. 8. The results showed that the two WS-derived

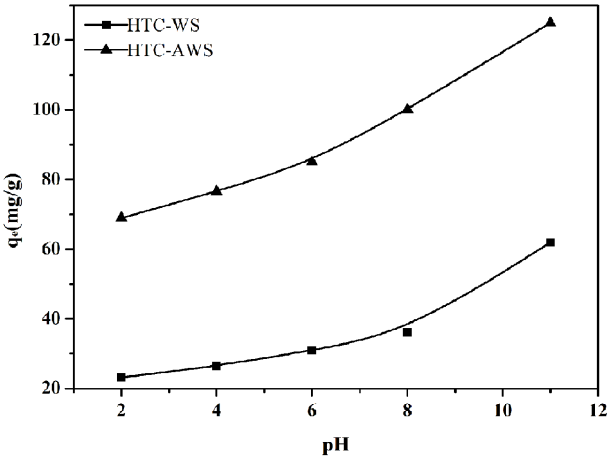

Fig. 6. Effect of solution initial pH on MB adsorption onto walnut shell-derived hydrochars (dose, 0.02 g; contact time, 300 min; C_0, 50 mg/L for HTC-WS, 100 mg/L for HTC-AWS).

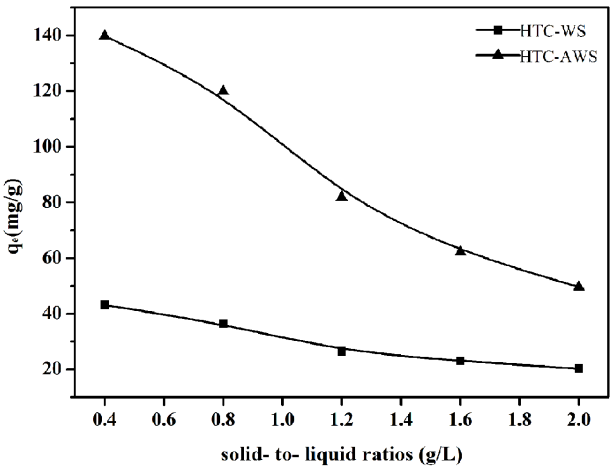

Fig. 7. Effect of adsorbent dosage on MB adsorption onto walnut shell-derived hydrochars (pH, 7 ± 0.5; contact time, 300 min; C_0, 50 mg/L for HTC-WS, 100 mg/L for HTC-AWS).

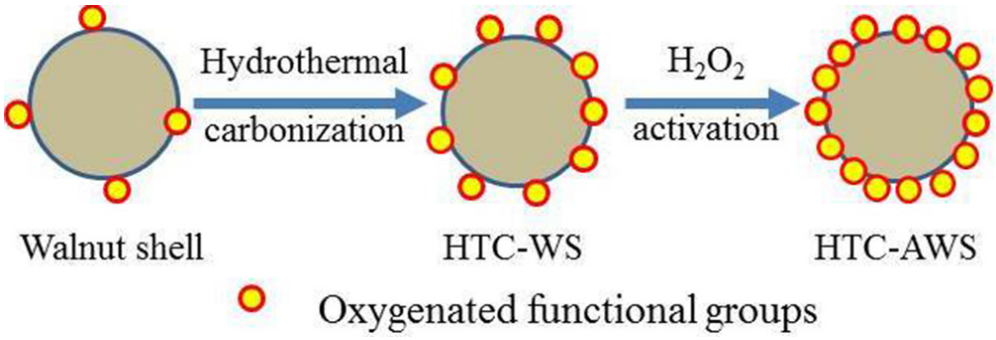

Fig. 5. Formation of oxygenated functional groups during hydrothermal carbonization and H_2O_2 activation.

hydrochars adsorption MB process was similar, which consisted of two phases: a primary rapid phase and a secondary slow phase [35]. At the first 100 min, MB removal was in the rapid phase, and about 85% of the maximal capacity was achieved. This quite rapid removal was due to the concentration gradient of MB and more available sites at the beginning of the adsorption process. From 100 to 360 min, the adsorption of MB gradually decreased with time until saturation was attained. At the second phase of MB uptake, the active sites of the WS-hydrochars were occupied by MB, which reduced the adsorption sites [36]. The reason for the adsorption behavior slowed down in later stage also was the repulsive forces between the solute molecules of the solid and bulk phase [35], so that the remaining adsorption sites may be difficult to occupy. The two-stage sorption mechanisms with the first rapid and quantitatively predominant and the second slower and quantitatively insignificant was consistent with literature [37].

Two kinetic models including pseudo-first-order and the pseudo-second-order were used to estimate the kinetic parameters. The two models basically considering external film diffusion, intraparticle diffusion and interaction step for adsorption process. The rate determining step of adsorption reaction may be one of the above three steps [38]. The pseudo-first-order model and the pseudo-second-order model is expressed as shown in Eq, (2) [39] and Eq. (3) [40], respectively.

$$\log\left(q_e - q_t\right) = \log q_e - \frac{k_1 t}{2.303} \tag{2}$$

$$\frac{t}{q_t} = \frac{1}{k_2 q_e^{\,2}} + \frac{t}{q_e} \tag{3}$$

where q_e and q_t are the amounts of MB adsorbed (mg·g^{-1}) at equilibrium and at time t (min), k_1 is the pseudo-first-order rate constant (min^{-1}); where k_2 (g mg^{-1} min^{-1}) is the rate constant of the pseudo-second-order adsorption.

The pseudo-first and pseudo-second order kinetic models are fitted in Fig. 8. The model fitting parameters describing MB adsorption onto hydrochars are presented in Table 3. The fitting results showed that the kinetic parameters of two WS-hydrochars adsorption MB were consistent. For the pseudo-first-order model, although it showed slightly fitting to the experimental data with the correlation coefficients more than 0.88, the calculated equilibrium adsorption capacities ($q_{e,\mathrm{cal}}$) deviated largely from the experimental values ($q_{e,\mathrm{exp}}$). In contrast, the high correlation coefficients ($R^2 > 0.99$) were obtained by the pseudo-second-order model, and the agreement between the $q_{e,\mathrm{cal}}$ achieved from the model and the experimental values ($q_{e,\mathrm{exp}}$) were evaluated. These results demonstrated that the pseudo-second-order model was suitable for characterizing the kinetic data. This observation indicated that the adsorption rate was dependent on the accessibility of the adsorption sites rather than the concentration of the MB in the solution [3]. Comparing of k_2 values indicated that the adsorption of MB onto HTC-WS was faster than on HTC-AWS, which could be attributed to the more uniform and simple surface structure of the HTC-WS.

Langmuir and Freundlich isotherm models were applied to analyze the relationship between equilibrium concentration and adsorbed amount of MB dye by HTC-WS and

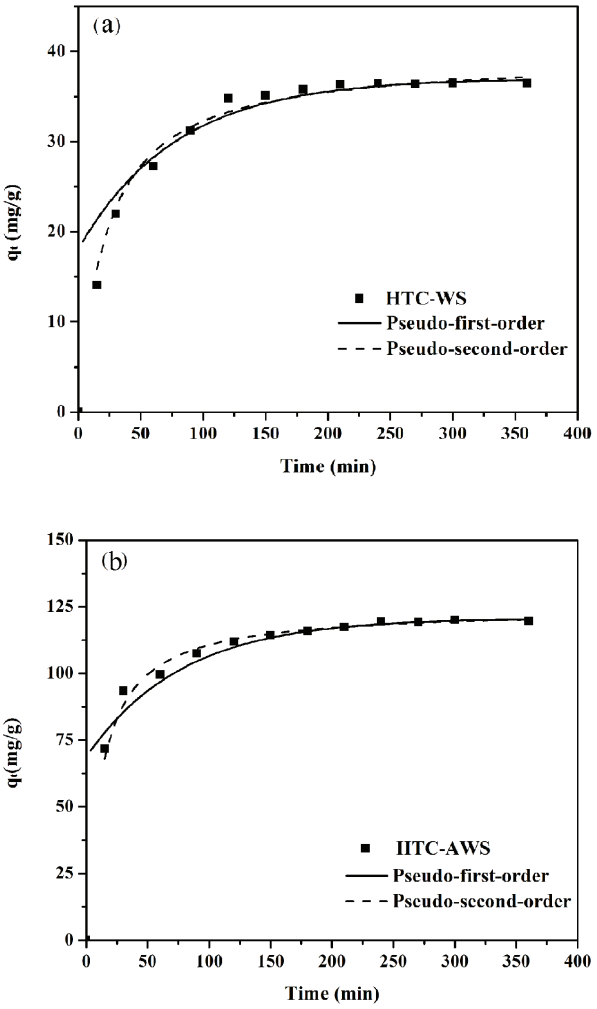

Fig. 8. Adsorption kinetics data and modeling for MB onto (a) HTC-WS and (b) HTC-AWS (pH, 7 ± 0.5; dose, 0.02 g; C_0, 50 mg/L for HTC-WS, 100 mg/L for HTC-AWS).

Table 3
Adsorption kinetic parameters of MB adsorption onto walnut shell-derived hydrochars

Sample	Pseudo-first-order				Pseudo-second-order		
	k_1 (min^{-1})	$q_{e',\mathrm{cal}}$ (mg/g)	$q_{e,\mathrm{exp}}$ (mg/g)	R^2	k_2 (g/(mg·min))	$q_{e,\mathrm{cal}}$ (mg/g)	R^2
HTC-WS	0.0128	18.94	37.01	0.88335	0.0011	39.53	0.9984
HTC-AWS	0.0129	52.18	120.84	0.92133	0.0006	124.38	0.9997

HTC-AWS. The Langmuir isotherm portrays adsorption on the homogeneous surface with monolayer adsorption systems. By contrast, the Freundlich isotherm describes the adsorption process on heterogeneous surfaces [3]. The Langmuir and Freundlich isotherms were expressed by the following equations [41,42], respectively:

$$\frac{C_e}{q_e} = \frac{1}{bq_m} + \frac{C_e}{q_m} \tag{4}$$

$$\log q_e = \log K_f + \frac{1}{n}\log C_e \tag{5}$$

where constant b is related to the energy of adsorption (L/mg), q_m is the maximum adsorption capacity (mg/g), K_f is roughly an indicator of the adsorption capacity and $1/n$ is the adsorption intensity.

The adsorption isotherm indicates how the adsorption molecules distribute between the liquid phase and the solid phase when the adsorption process reaches an equilibrium state. The analysis of the isotherm data by fitting them to different isotherm models is an important step to find the suitable model that can be used for design purpose [43]. Experimental data of MB adsorption onto these two hydrochars and the fitting results by Langmuir and Freundlich models are shown in Fig. 9. The adsorption isotherm parameter values including q_m, K_L, K_f, and $1/n$ as well as the correlation coefficients R^2 for MB presented in Table 4. As Table 4 shows, the values of R^2 of the Langmuir model for the HTC-WS and HTC-AWS were 0.9811 and 0.9970, the values of R^2 of the Freundlich model were 0.9680 and 0.9301, respectively. Therefore, the adsorption of MB onto the HTC-WS and HTC-AWS could be described by both Langmuir and Freundlich models, while Langmuir model was slightly better. This indicated that the characteristic of adsorption should be monolayer adsorption process of MB onto the HTC-WS and HTC-AWS with the corresponding monolayer saturated adsorption capacity of 50.56, and 173.92 mg/g, respectively.

The favorability of MB adsorption onto WS-derived hydrochars could be evaluated based on the Langmuir isotherm from dimensionless constant called separation factor or equilibrium factor (R_L). $R_L = 1/(1 + C_0 b)$, where C_0 is the initial MB concentration. The value of R_L mean the irreversible adsorption ($R_L = 0$), favorable adsorption ($0 < R_L < 1$), linear adsorption ($R_L = 1$), unfavorable adsorption ($R_L > 1$) [33,44]. In this work, as shown in Fig. 10, R_L was less than 1 and suggested that the adsorption of MB onto WS-derived hydrochar was favorable. Furthermore, increasing the initial MB concentration promoted the adsorption process. The factor $1/n$ in the Freundlich isotherm model can also reflect the complexity of adsorption process. Values of $1/n$ smaller than 0.5 indicates that the adsorbate is easily adsorbed; values of $1/n$ larger than 2 indicates the adsorbate is hardly adsorbed [33]. The $1/n$ values of MB onto the HTC-WS were calculated to be 0.21498, which implied that the adsorption of MB onto HTC-WS was favorable. On the other hand, the $1/n$ values (0.17913) of MB on the HTC-AWS were lower than HTC-WS, which indicated the easier adsorption of MB on the hydrochars activation with H_2O_2 and these results might also be attributed to the possibly stronger hydrogen bonds formed between MB and HTC-AWS [19].

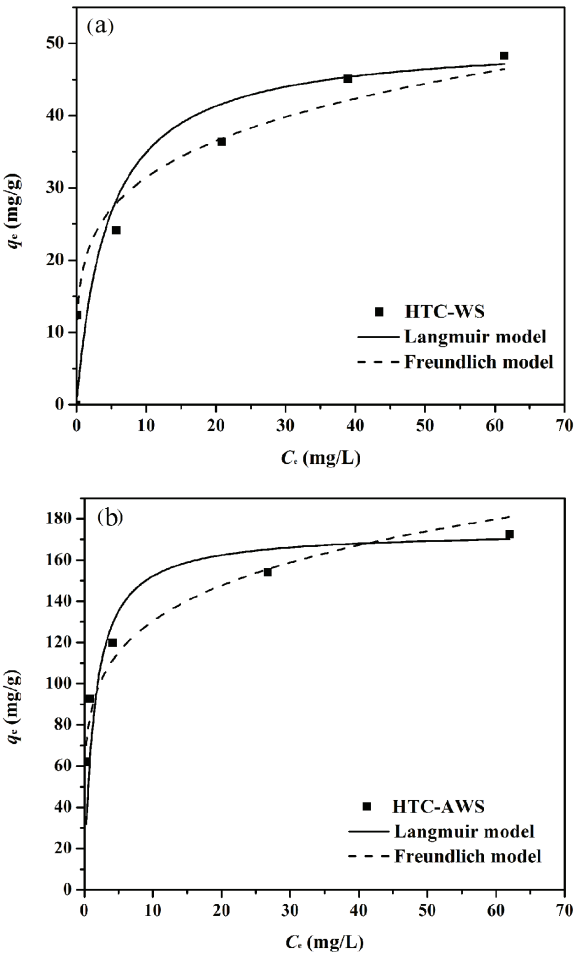

Fig. 9. Equilibrium adsorption isotherms of MB onto (a) HTC-WS and (b) HTC-AWS (pH, 7 ± 0.5; dose, 0.02 g; contact time, 300 min).

Table 4
Adsorption isotherm parameters of MB adsorption onto walnut shell-derived hydrochars

Sample	Langmuir equation			Freundlich equation		
	q_m (mg·g^{-1})	b (L·mg^{-1})	R^2	K_f (mg·g^{-1})	$1/n$	R^2
HTC-WS	50.56	0.2236	0.9811	19.17	0.21498	0.9680
HTC-AWS	173.92	0.6970	0.9970	86.35	0.17913	0.9301

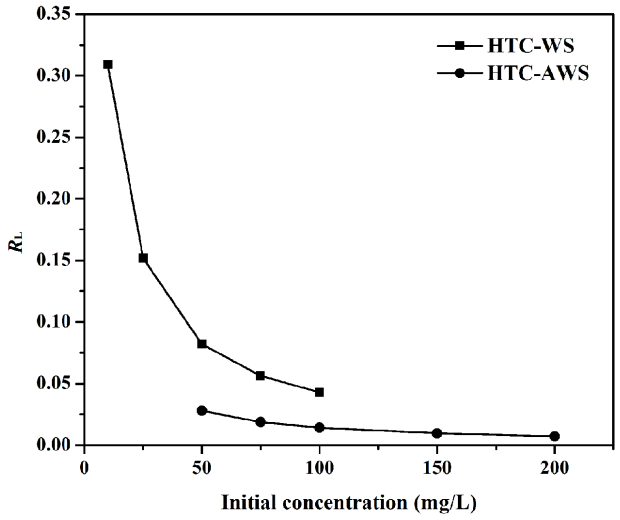

Fig. 10. Effect of initial MB concentration on the Langmuir equilibrium factor (R_L) for adsorption onto walnut shell-derived hydrochars.

3.3. Adsorption mechanisms

The mechanisms of adsorption MB onto HTC-WS and HTC-AWS were significantly different compared with the biochars which depended on the physical adsorption. The molecule of MB is aromatic and non-polar, and contains a positively charged amine group [12]. Therefore, molecular electrostatic interactions can occur in an adsorption process due to the negative charge of WS-derived hydrochar surface and the ionization of the MB in solution, which was governed by the solution pH. The possible mechanisms were π–π interaction between the MB cation and the hydrochar with electrons of C=C [1,13]. This was confirmed by zeta potentials and FT-IR analysis of hydrochars. H_2O_2 was used to oxidize HTC-WS surfaces and increase oxygen-containing surface functional groups, particularly carboxylic group, which enhanced electrostatic interactions between MB^+ and hydrochars and increased the adsorption capability of hydrochar. Van der Waals attraction forces may also be significant for adsorption of MB by HTC-WS and HTC-AWS, although HTC-WS and HTC-AWS had low BET surface area and pore volume. The functional groups of WS-derived hydrochar such as –COOH and $–NH_2$ can also act as hydrogen-bonding donors and form hydrogen bonds with MB. In general, the MB adsorption mechanism was complex which might involve complex interaction of physical and chemical factors.

4. Conclusions

The ability of HTC-WS and HTC-AWS to remove MB from aqueous solutions was evaluated in batch mode examining the influence of initial pH value, adsorbent dose, contact time and initial MB solution concentrations. It was found that the increase of MB removal using H_2O_2-activated HTC-WS rose threefold compared with untreated HTC-WS. The results of FT-IR, zeta potentials, SEM and pore size distributions analysis of both, HTC-WS and HTC-AWS, showed structural changes which might affect the increase of the MB sorption following H_2O_2 treatment. The adsorption equilibrium data were best fitted by the Langmuir isotherm model and the adsorption kinetics followed pseudo-second-order models for both HTC-WS and HTC-AWS. The main mechanism of adsorption MB onto HTC-WS and HTC-AWS depended on molecular electrostatic interactions. The obtained WS-derived hydrochars were promising adsorbents for removal of MB from aqueous solution over a wide range of concentrations. Furthermore, WS-derived hydrochars as a waste product also resolved waste management issues. This paper provides important information for the high value conversion of waste biomass materials. HTC of the other waste biomass materials and their H_2O_2-activated form were worthy of further investigation.

Acknowledgments

Financial supports from National Natural Science Foundation of China (Grant No. 50804039), Educational commission of Sichuan Province of China (Grant No. 14ZB0106), Science and Technology Support Program of Sichuan Province of China (Grant No. 2016GZ0308) and the Platform Fund of Southwest University of Science and Technology (Grant No. 14tdgk04) were acknowledged. Analytical and testing center of Southwest University of Science and Technology was also acknowledged.

References

[1] G.K. Parshetti, S. Chowdhury, R. Balasubramanian, Hydrothermal conversion of urban food waste to chars for removal of textile dyes from contaminated waters, Bioresour. Technol., 161 (2014) 310–319.
[2] F.L. Braghiroli, V. Fierro, M.T. Izquierdo, J. Parmentier, A. Pizzi, A. Celzard, Kinetics of the hydrothermal treatment of tannin for producing carbonaceous microspheres, Bioresour. Technol., 151 (2014) 271–277.
[3] M.A. Islam, A. Benhouria, M. Asif, B.H. Hameed, Methylene blue adsorption on factory-rejected tea activated carbon prepared by conjunction of hydrothermal carbonization and sodium hydroxide activation processes, J. Taiwan Inst. Chem. Eng., 52 (2015) 57–64.
[4] A. Jain, R. Balasubramanian, M.P. Srinivasan, Production of high surface area mesoporous activated carbons from waste biomass using hydrogen peroxide-mediated hydrothermal treatment for adsorption applications, Chem. Eng. J., 273 (2015) 622–629.
[5] M. Sevilla, A.B. Fuertes, The production of carbon materials by hydrothermal carbonization of cellulose, Carbon, 47 (2009) 2281–2289.
[6] S. Kang, X. Li, J. Fan, J. Chang, Characterization of hydrochars produced by hydrothermal carbonization of lignin, cellulose, D-xylose, and wood meal, Ind. Eng. Chem. Res., 51 (2012) 9023–9031.
[7] A. Jain, R. Balasubramanian, M.P. Srinivasan, Hydrothermal conversion of biomass waste to activated carbon with high porosity: a review, Chem. Eng. J., 283 (2016) 789–805.
[8] K. Sun, K. Ro, M. Guo, J. Novak, H. Mashayekhi, B. Xing, Sorption of bisphenol A, 17α-ethinyl estradiol and phenanthrene on thermally and hydrothermally produced biochars, Bioresour. Technol., 102 (2011) 5757–5763.
[9] K. Sun, B. Gao, K.S. Ro, J.M. Novak, Z. Wang, S. Herbert, B. Xing, Assessment of herbicide sorption by biochars and organic matter associated with soil and sediment, Environ. Pollut., 163 (2012) 167–173.
[10] B. Chen, Z. Chen, Sorption of naphthalene and 1-naphthol by biochars of orange peels with different pyrolytic temperatures, Chemosphere, 76 (2009) 127–133.

[11] C. Falco, J.P. Marco-Lozar, D. Salinas-Torres, E. Morallón, D. Cazorla-Amorós, M.M. Titirici, D. Lozano-Castelló, Tailoring the porosity of chemically activated hydrothermal carbons: influence of the precursor and hydrothermal carbonization temperature, Carbon, 62 (2013) 346–355.
[12] M.D. Huff, J.W. Lee, Biochar-surface oxygenation with hydrogen peroxide, J. Environ. Manage., 165 (2016) 17–21.
[13] J.T. Petrović, M.D. Stojanović, J.V. Milojković, M.S. Petrović, T.D. Šoštarić, M.D. Laušević, M.L. Mihajlović, Alkali modified hydrochar of grape pomace as a perspective adsorbent of Pb^{2+} from aqueous solution, J. Environ. Manage., 182 (2016) 292–300.
[14] Y. Xue, B. Gao, Y. Yao, M. Inyang, M. Zhang, A.R. Zimmerman, K.S. Ro, Hydrogen peroxide modification enhances the ability of biochar (hydrochar) produced from hydrothermal carbonization of peanut hull to remove aqueous heavy metals: batch and column tests, Chem. Eng. J., 200–202 (2012) 673–680.
[15] M.A. Islam, M.J. Ahmed, W.A. Khanday, M. Asif, B.H. Hameed, Mesoporous activated carbon prepared from NaOH activation of rattan (*Lacosperma secundiflorum*) hydrochar for methylene blue removal, Ecotoxicol. Environ. Saf., 138 (2017) 279–285.
[16] P. Regmi, J.L. Garcia Moscoso, S. Kumar, X. Cao, J. Mao, G. Schafran, Removal of copper and cadmium from aqueous solution using switchgrass biochar produced via hydrothermal carbonization process, J. Environ. Manage., 109 (2012) 61–69.
[17] K. Sun, J. Tang, Y. Gong, H. Zhang, Characterization of potassium hydroxide (KOH) modified hydrochars from different feedstocks for enhanced removal of heavy metals from water, Environ. Sci. Pollut. Res., 22 (2015) 16640–16651.
[18] X. Zuo, Z. Liu, M. Chen, Effect of H_2O_2 concentrations on copper removal using the modified hydrothermal biochar, Bioresour. Technol., 207 (2016) 262–267.
[19] Y. Li, A. Meas, S. Shan, R. Yang, X. Gai, Production and optimization of bamboo hydrochars for adsorption of Congo red and 2-naphthol, Bioresour. Technol., 207 (2016) 379–386.
[20] W. Bae, J. Kim, J. Chung, Production of granular activated carbon from food-processing wastes (walnut shells and jujube seeds) and its adsorptive properties, J. Air Waste Manage. Assoc., 64 (2014) 879–886.
[21] Y. Kar, Co-pyrolysis of walnut shell and tar sand in a fixed-bed reactor, Bioresour. Technol., 102 (2011) 9800–9805.
[22] E.I. Pujol Pereira, E.C. Suddick, J. Six, Carbon abatement and emissions associated with the gasification of walnut shells for bioenergy and biochar production, PLoS One, 11 (2016) e0150837.
[23] H.H. Hammud, A. Shmait, N. Hourani, Removal of Malachite Green from water using hydrothermally carbonized pine needles, RSC Adv., 5 (2015) 7909–7920.
[24] M. Ghaedi, H. Mazaheri, S. Khodadoust, S. Hajati, M.K. Purkait, Application of central composite design for simultaneous removal of methylene blue and Pb^{2+} ions by walnut wood activated carbon, Spectrochim. Acta Part A, 135 (2015) 479–490.
[25] L. Trakal, R. Šigut, H. Šillerová, D. Faturíková, M. Komárek, Copper removal from aqueous solution using biochar: effect of chemical activation, Arabian J. Chem., 7 (2014) 43–52.
[26] E. Unur, Functional nanoporous carbons from hydrothermally treated biomass for environmental purification, Microporous Mesoporous Mater., 168 (2013) 92–101.
[27] R. Xie, H. Wang, Y. Chen, W. Jiang, Walnut shell-based activated carbon with excellent copper (II) adsorption and lower chromium (VI) removal prepared by acid-base modification, Environ. Prog. Sustain. Energy, 32 (2013) 688–696.
[28] J.C. Tanger, K.S. Pitzer, Calculation of the ionization constant of H_2O to 2273 K and 500 MPa, AIChE J., 35 (1989) 1631–1638.
[29] F.S. Asghari, H. Yoshida, Acid-catalyzed production of 5-hydroxymethyl furfural from D-fructose in subcritical water, Ind. Eng. Chem. Res., 45 (2006) 2163–2173.
[30] S.H. Wang, P.R. Griffiths, Resolution enhancement of diffuse reflectance Ir spectra of coals by Fourier self-deconvolution: 1. C-H stretching and bending modes, Fuel, 64 (1985) 229–236.
[31] H. Li, Y. Yang, S. Yang, A. Chen, D. Yang, Infrared spectroscopic study on the modified mechanism of aluminum-impregnated bone charcoal, J. Spectrosc., 2014 (2014) 1–7.
[32] B.H. Hameed, D.K. Mahmoud, A.L. Ahmad, Sorption equilibrium and kinetics of basic dye from aqueous solution using banana stalk waste, J. Hazard. Mater., 158 (2008) 499–506.
[33] S. Fan, Y. Wang, Z. Wang, J. Tang, J. Tang, X. Li, Removal of methylene blue from aqueous solution by sewage sludge-derived biochar: adsorption kinetics, equilibrium, thermodynamics and mechanism, J. Environ. Chem. Eng., 5 (2017) 601–611.
[34] H. Yang, L. Weijun, W. Weiqing, F. Qiming, L. Jing, Synthesis of a carbon@ Rectorite nanocomposite adsorbent by a hydrothermal carbonization process and their application in the removal of methylene blue and neutral red from aqueous solutions, Desal. Wat. Treat., 57 (2016) 13573–13585.
[35] Y. Chen, J. Wang, Removal of radionuclide Sr^{2+} ions from aqueous solution using synthesized magnetic chitosan beads, Nucl. Eng. Des., 242 (2012) 445–451.
[36] S. Yeşim, A. Yücel, Mass transfer and equilibrium studies for the sorption of chromium ions onto chitin, Process Biochem., 36 (2000) 157–173.
[37] A. Saeed, M. Sharif, M. Iqbal, Application potential of grapefruit peel as dye sorbent: kinetics, equilibrium and mechanism of crystal violet adsorption, J. Hazard. Mater., 179 (2010) 564–572.
[38] M. Monier, D.M. Ayad, A.A. Sarhan, Adsorption of Cu(II), Hg(II), and Ni(II) ions by modified natural wool chelating fibers, J. Hazard. Mater., 176 (2010) 348–355.
[39] S. Largegren, About the theory of so-called adsorption of soluble substances, K. Sven. Vetenska.akad. Handl., 24 (1989) 1–39.
[40] Y.S. Ho, G. McKay, Pseudo-second order model for sorption processes, Process Biochem., 34 (1999) 451–465.
[41] H.M.F. Freundlich, On the adsorption in solution, J. Phys. Chem., 57 (1906) 385–471.
[42] I. Langmuir, The constitution and fundamental properties of solids and liquids. Part I. Solids, J. Am. Chem. Soc., 38 (1916) 2221–2295.
[43] M.S. El-Geundi, Homogeneous surface diffusion model for the adsorption of basic dyestuffs onto natural clay in batch adsorbers, Adsorpt. Sci. Technol., 8 (1991) 217–225.
[44] H. Faghihian, M. Moayed, A. Firooz, M. Iravani, Synthesis of a novel magnetic zeolite nanocomposite for removal of Cs^{+} and Sr^{2+} from aqueous solution: kinetic, equilibrium, and thermodynamic studies, J. Colloid Interface Sci., 393 (2013) 445–451.